Topics in Magnetic Resonance Imaging

Investigating the Vascular Phenotype of Subcutaneously and Orthotopically Propagated PC3 Prostate Cancer Xenografts Using Combined Carbogen USPIO (CUSPIO) MRI

--Manuscript Draft--

Manuscript Number:	TMRI-16-00016R1
Full Title:	Investigating the Vascular Phenotype of Subcutaneously and Orthotopically Propagated PC3 Prostate Cancer Xenografts Using Combined Carbogen USPIO (CUSPIO) MRI
Article Type:	Invited Review Article
Keywords:	Tumour; vasculature; USPIO; drug delivery
Corresponding Author:	Simon P Robinson, PhD Institute of Cancer Research UNITED KINGDOM
Corresponding Author Secondary Information:	
Corresponding Author's Institution:	Institute of Cancer Research
Corresponding Author's Secondary Institution:	
First Author:	Jake S Burrell, PhD
First Author Secondary Information:	
Order of Authors:	Jake S Burrell, PhD
	Simon Walker-Samuel, PhD
	Jessica KR Boult, PhD
	Lauren CJ Baker, PhD
	Yann Jamin, PhD
	Jane Halliday, PhD
	John C Waterton, PhD
	Simon P Robinson, PhD
Order of Authors Secondary Information:	
Manuscript Region of Origin:	UNITED KINGDOM
Abstract:	Objectives: To use the combined carbogen USPIO (CUSPIO) MRI method, which uses spatial correlations in independent susceptibility imaging biomarkers, to investigate and compare the impact of tumour size and anatomical site on vascular structure and function in vivo. Methods: Mice bearing either subcutaneous or orthotopic PC3 LN3 prostate tumours were imaged at 7T, using a multi-gradient echo sequence to quantify R2*, prior to and during carbogen (95% O2/5% CO2) breathing, and subsequently following intravenous administration of ultrasmall superparamagnetic iron oxide (USPIO) particles. Carbogen and USPIO-induced changes in R2* were used to inform on haemodynamic vasculature and fractional blood volume (%) respectively. The CUSPIO imaging data were also segmented to identify and assess six categories of R2* response. Results: Small and large subcutaneous and orthotopic tumour cohorts all exhibited significantly ($p<0.05$) different median baseline R2*, R2*carbogen and fractional blood volume.

	CUSPIO imaging showed small subcutaneous tumours predominantly exhibited a negative R2*carbogen followed by a positive R2*USPIO, consistent with a well perfused tumour vasculature. Large subcutaneous tumours exhibited a small positive R2*carbogen and relatively low fractional blood volume, suggesting less functional vasculature. Orthotopic tumours revealed a large, positive R2*carbogen, consistent with vascular steal, and which may indicate that vascular function is more dependent on site of implantation than tumour size. Regions exhibiting significant R2*carbogen, but no significant R2*USPIO, suggesting transient vascular shutdown over the experimental timecourse, were apparent in all three cohorts. Conclusions: CUSPIO imaging can inform on efficient drug delivery via functional vasculature in vivo, and on appropriate tumour model selection for pre-clinical therapy trials

Cancer Research UK Cancer Imaging Centre
Division of Radiotherapy & Imaging

Directors:
Professor Martin Leach
Professor Nandita deSouza

Dr. Marie-France Penet
Guest Editor
Topics in Magnetic Resonance Imaging

20th July 2016

Dear Marie-France,

Thankyou for your positive comments on our manuscript, “Investigating the Vascular Phenotype of Subcutaneously and Orthotopically Propagated PC3 Prostate Cancer Xenografts Using Combined Carbogen USPIO (CUSPIO) MRI”, MS# TMRI-16-00016.

Please find below our point-by-point responses to your minor comments you raised. Revisions are in red text in the revised marked manuscript.

We hope that the manuscript is now acceptable for publication in Topics in Magnetic Resonance Imaging.

Yours faithfully,

Simon Robinson

The Institute of Cancer Research

Simon P. Robinson Ph.D
Team Leader – Magnetic Resonance
CR-UK Cancer Imaging Centre
Division of Radiotherapy & Imaging
Cotswold Road
Sutton SM2 5NG
Surrey UK
Tel: +44 0208 722 4528
Email: Simon.Robinson@icr.ac.uk

Registered office
The Institute of Cancer Research:
Royal Cancer Hospital
123 Old Brompton Road
London SW7 3RP

A Charity. Not for Profit.
Company Limited by Guarantee.
Registered in England No. 534147.
VAT Registration No. 849 0581 02

Could you please check the abbreviations. Please define when used first (USPIO in introduction, TE, TR, AQ…)

- *Abbreviations have been checked and defined as requested.*

Could you please add more details about the PC3 LN3 cells?

- *Detail on the origins of the PC3 LN3 cells, and relevant literature, have been added to the Methods section.*

How does the dental paste (page 5) limit animal motion?

- *Dental paste was used to limit any respiratory-associated motion artefacts. The word "respiratory" has been added to clarify this.*

If possible, could you please add the corresponding anatomic images to the maps to delineate the tumors in Figure 2?

- *This is difficult, as the CUSPIO maps have been re-sized/expanded to emphasise the distribution of the different response categories measured between the small and large subcutaneous tumours, and the orthotopic PC3 tumours.*

Page 8 - CD31 fluorescent microscopy is mentioned in the title of a section, but there are no results with CD31 staining.

- *The section title has been amended with reference to CD31 staining deleted.*

Penet *et al* have observed differences in vascular volume between orthotopic and subcutaneous PC3 xenografts. Could the authors please include this previous observation in their discussion?

- *This observation and the associated citation have now been added to the Discussion.*

The representative Hoechst staining images do not clearly demonstrate significant differences mentioned in the summarized data – could the authors select images that reflect the overall differences.

- *The Hoechst 33342 images were deliberately chosen as they represent individual data closest to the mean Hoechst 33342 perfused area determined for each tumour size/site. The uploaded tiff files do show the pattern described in the text – perhaps there has been some corruption of the images in generating the merged pdf file of the whole manuscript?*

Could the authors please expand upon why the small subcutaneous tumors have the highest vascular volume but are most hypoxic.

- *The thinking here is that small tumours initially develop a functional vasculature capable of providing nutritive blood supply, but which does not meet the evolving metabolic adaptation/demands of the cancer cells, hence their markedly elevated hypoxia. This has now been incorporated into the Discussion.*

Investigating the Vascular Phenotype of Subcutaneously and Orthotopically Propagated PC3 Prostate Cancer Xenografts Using Combined Carbogen USPIO (CUSPIO) MRI

Jake S. Burrell[1], PhD, Simon Walker-Samuel[1,2], PhD, Jessica K.R. Boult[1], PhD, Lauren C.J. Baker[1], PhD, Yann Jamin[1], PhD, Jane Halliday[3], PhD, John C. Waterton[3#], PhD, Simon P. Robinson[1], PhD

[1]Cancer Research UK Cancer Imaging Centre, Division of Radiotherapy and Imaging, The Institute of Cancer Research, 15 Cotswold Road, Sutton, Surrey, SM2 5NG, UK.

[2]Centre for Advanced Biomedical Imaging, Department of Medicine and Institute of Child Health, University College London, 72 Huntley Street, London, WC1E 6DD, UK.

[3]R&D Personalised Healthcare & Biomarkers, AstraZeneca, Alderley Park, Macclesfield, SK10 4TG, UK.

Corresponding Author:

Simon Robinson
Cancer Research UK Cancer Imaging Centre
Division of Radiotherapy & Imaging
The Institute of Cancer Research
15 Cotswold Rd
Sutton
Surrey
SM2 5NG

Tel: 020 8722 4528
Fax: 020 8661 0846
Simon.Robinson@icr.ac.uk

[#]Present address: Centre for Imaging Sciences
Stopford Building
Oxford Road
University of Manchester
Manchester M13 9PT
UK

Grant Support:

This work was supported by a BBSRC/AstraZeneca Industrial Partnership Studentship (grant number BB/E528979/1), the Medical Research Council (grant G0700017) and AstraZeneca. We gratefully acknowledge the support received for the Institute of Cancer Research Cancer Research UK & EPSRC Cancer Imaging Centre, in association with the MRC and Department of Health (England) (grant C1060/A10334) and NHS funding to the NIHR Biomedical Research Centre.

Running Title: CUSPIO imaging of subcutaneous and orthotopic tumours

Abstract

Objectives:

To use the combined carbogen USPIO (CUSPIO) MRI method, which uses spatial correlations in independent susceptibility imaging biomarkers, to investigate and compare the impact of tumour size and anatomical site on vascular structure and function *in vivo*.

Methods:

Mice bearing either subcutaneous or orthotopic PC3 LN3 prostate tumours were imaged at 7T, using a multi-gradient echo sequence to quantify R_2*, prior to and during carbogen (95% O_2/5% CO_2) breathing, and subsequently following intravenous administration of ultrasmall superparamagnetic iron oxide (USPIO) particles. Carbogen and USPIO-induced changes in R_2* were used to inform on haemodynamic vasculature and fractional blood volume (%) respectively. The CUSPIO imaging data were also segmented to identify and assess six categories of R_2* response.

Results:

Small and large subcutaneous and orthotopic tumour cohorts all exhibited significantly ($p<0.05$) different median baseline R_2*, $\Delta R_2^*_{carbogen}$ and fractional blood volume. CUSPIO imaging showed small subcutaneous tumours predominantly exhibited a negative $\Delta R_2^*_{carbogen}$ followed by a positive $\Delta R_2^*_{USPIO}$, consistent with a well perfused tumour vasculature. Large subcutaneous tumours exhibited a small positive $\Delta R_2^*_{carbogen}$ and relatively low fractional blood volume, suggesting less functional vasculature. Orthotopic tumours revealed a large, positive $\Delta R_2^*_{carbogen}$, consistent with vascular steal, and which may indicate that vascular function is more dependent on site of implantation than tumour size. Regions exhibiting significant $\Delta R_2^*_{carbogen}$, but no significant $\Delta R_2^*_{USPIO}$, suggesting transient vascular shutdown over the experimental timecourse, were apparent in all three cohorts.

Conclusions:

CUSPIO imaging can inform on efficient drug delivery via functional vasculature *in vivo*, and on appropriate tumour model selection for pre-clinical therapy trials

Keywords: Tumour, vasculature, USPIO, drug delivery

Introduction

The combined carbogen USPIO imaging protocol (CUSPIO) combines two magnetic resonance imaging (MRI) techniques, intrinsic susceptibility contrast MRI and contrast enhanced susceptibility MRI with ultra small super paramagnetic iron oxide (USPIO) particles. The transverse relaxation rate (R_2*) slows with high oxygen-content gas breathing, which decreases the ratio of deoxyhaemoglobin (paramagnetic) to oxyhaemoglobin (diamagnetic) in blood. The resulting change in R_2*, $\Delta R_2^*_{carbogen}$, reflects changes in oxygenation and the haemodynamic response in functional vasculature. Intravenous injection of USPIO particles increases R_2* in tissue surrounding blood vessels that are perfused with blood plasma at the time of injection. With a known blood concentration of USPIO particles, $\Delta R_2^*_{USPIO}$ can be used to calculate fractional blood volume. Given the difference in size of erythrocytes and USPIO particles, (~6μm and 0.03μm, respectively (1)), the volume of distribution influenced by hyperoxia and USPIO is likely to differ, with small vessels offering preferential access to USPIO particles. By combining, into a single imaging session, sequential measurements of ΔR_2* induced by carbogen breathing and USPIO particles, greater information about vascular function and structure can be deduced than could be achieved using each technique individually (2). The CUSPIO protocol achieves this by implementing a novel segmentation scheme, in which ΔR_2* estimates are compared and assigned to one of five response categories. Our previous work has shown that these categories provide distinct information about vascular function, the spatial distribution of plasma perfusion and transient hypoxia, and that these biomarkers can inform on tumour response to anti-angiogenic therapy (2, 3).

The clinical relevance of rodent models in both fundamental cancer research and drug development has been an ongoing debate for many years. The inadequacies and limitations of ectopic (subcutaneous) models are frequently highlighted, but there has also been a historical reluctance to adopt more complex models in cancer research (4-6). Today, more sophisticated orthotopically propagated tumour models, in which cancer cells are implanted and grown within the organ from which they were derived, and genetically-engineered mouse (GEM) models, in which tumours are driven by the expression of the target of interest and arise spontaneously within the native tissue of origin, are being increasingly exploited (7, 8). These models more faithfully emulate human tumour growth, tumour-host stromal interactions and vasculature, metastatic potential and therapeutic response *in vivo*. The systematic use of orthotopic and GEM models in pre-clinical cancer research demands non-invasive anatomical and functional imaging methods for the longitudinal monitoring of tumour progression and response, which can also accurately inform on key hallmarks of cancer,

such as angiogenesis. We have previously demonstrated the use of several MRI strategies with which to assess, and reveal differences, in the vascular phenotype and response of ectopic, orthotopic and GEM models (9-15).

The purpose of this study was to exploit CUSPIO imaging to investigate vascular function and structure in small and large subcutaneous, and orthotopically propagated PC3 LN3 prostate xenografts, and compare the differences in these characteristics between the different models.

Materials and Methods

Cell Culture

Human PC3 LN3 prostate tumour cells, originally generated in-house from lymph node metastases arising in nude mice bearing orthotopic PC3 tumours (16), were cultured in T75 cm3 flasks (Corning Life Sciences) in Dubbecco's Modified Eagles Medium (DMEM; Invitrogen, Paisley, UK) supplemented with 10% (v/v) foetal bovine serum, 5mM L-glutamine,100IU/ml penicillin and 100µg/ml streptomycin (all Invitrogen). Cells were maintained at 37ºC in a humidified 5% CO_2 atmosphere.

Tumour Propagation

All experiments were performed in accordance with the local ethical review panel, the UK Home Office Animals (Scientific Procedures) Act 1986, the United Kingdom National Cancer Research Institute guidelines for animal welfare in cancer research (17), and the Animal Research: Reporting of *In Vivo* Experiments (ARRIVE) guidelines (18). Male NCr nude mice under isoflurane anaesthesia were injected with 1×10^6 PC3 LN3 cells subcutaneously on the right flank, or 1×10^5 cells into the ventral prostate gland (9). The subcutaneously inoculated animals were randomised into two groups of six mice, to be imaged as small and large tumours. Animals from group 1 were imaged one week later, and animals from group 2 were imaged three weeks later. Orthotopically inoculated animals were monitored by palpation and imaged after three weeks (n=5). No adverse effects were observed in any of the mice, and none excluded from the study.

Combined Carbogen-USPIO (CUSPIO) Imaging Protocol

Tumour-bearing mice were anaesthetised by an intraperitoneal injection of 10ml/kg of fentanyl citrate (0.315 mg/ml) plus fluanisone (10 mg/ml) (Hypnorm, Janssen Pharmaceutical, High Wycombe, UK), midazolam (5 mg/ml) (Hypnovel, Roche, Burgess Hill, UK), and sterile water (1:1:2). A lateral tail vein was cannulated with a 27G butterfly catheter

(Venisystems; Abbot Laboratories, Maidenhead, UK) for remote administration of USPIO particles. A nosepiece was positioned for delivery of air or carbogen (95% O_2/5% CO_2) at a flow rate of 1 L/min. During MRI, all mice were restrained using dental paste in order to limit respiratory motion artefacts (19). A warm air blower was used to maintain the animal's core temperature at 37ºC within the magnet bore.

MRI was performed on a 7T horizontal bore microimaging system (Bruker, Ettlingen, Germany) using a 3cm birdcage coil. T_2-weighted turboRARE images (echo time TE=36ms, repetition time TR=4200ms, 2 averages) were first acquired from contiguous 1mm thick axial slices for tumour localisation and volume determination. Next, two sets of multi gradient echo (MGE) images (TE=6-28ms, 4ms echo spacing, TR=200ms, flip angle α=45º, 8 averages, acquisition time AQ=3min37s) were acquired from three axial 1mm slices through the tumour centre whilst the mouse breathed air. The gas supply was then switched to carbogen, and following a ten minute transition period, a further identical MGE image set was acquired. The gas supply was then reverted back to air and, after another 10 minute transition period, another MGE image set was acquired. A final MGE image set was then acquired one minute after intravenous injection of 150μmol/kg USPIO particles (ferumoxtran-10, Sinerem, Guerbet, Villepinte, France).

Tumour volumes were determined using segmentation from regions of interest (ROI's) drawn on T_2-weighted images for each tumour-containing slice, using in-house software (Imageview, developed in IDL, ITT Visual Information Systems, Boulder, CO). MGE data were analysed using a Bayesian maximum *a posteriori* approach (20). This modelled the MGE signal magnitude as a single exponential decay and took into account its Rician distribution. Furthermore, it enabled estimates of ΔR_2^* uncertainty to be defined and the probability that a given ΔR_2^* estimate was significantly greater than or less than zero. Thus, the number of voxels within the tumour ROI with an uncertainty of less than $0.05ms^{-1}$ and with a significant ($p<0.05$) change in R_2^* induced by carbogen ($\Delta R_2^*_{carbogen}$) and/or USPIO particles ($\Delta R_2^*_{USPIO}$) were calculated. Fractional blood volume (ξ, %) was quantified from the $\Delta R_2^*_{USPIO}$ data as previously described (21). The increase in blood susceptibility caused by the USPIO particles was extrapolated from a previously published value for a dose of 200μmol/kg (22).

RGB maps were then generated, with the red channel designated to voxels with a positive $\Delta R_2^*_{carbogen}$, the blue channel to voxels with negative $\Delta R_2^*_{carbogen}$ and the green channel to positive $\Delta R_2^*_{USPIO}$. It was assumed that $\Delta R_2^*_{USPIO}$ could only be positive, and negative

values were assumed to be a result of uncertainty in R_2* estimates. Regions with both negative $\Delta R_2^*_{carbogen}$ and positive $\Delta R_2^*_{USPIO}$ therefore appeared cyan (blue + green), and regions with both positive $\Delta R_2^*_{carbogen}$ and positive $\Delta R_2^*_{USPIO}$ appeared yellow (red + green).

Histological Assessment of Tumour Perfusion

Following MRI, Hoechst 33342 (15mg/kg in water, Sigma, Poole, UK) was administered intravenously via a lateral tail vein. Hoechst 33342 is a nuclear dye that stains the cells lining blood vessels that are perfused at the time of injection, affording a measure of functional tumour vasculature (23). Mice were killed one minute after injection of Hoechst 33342 and tumours rapidly excised and snap frozen over liquid nitrogen. Contiguous 10μm frozen sections at 3 levels through each tumour were cut on a cryotome in approximately the same plane as was imaged with MRI. Sections were fixed in ice-cold acetone for 10 minutes before being mounted in phosphate buffered saline. Hoechst 33342 fluorescence signals from whole tumour sections were then recorded at 365nm using a motorized scanning stage (Prior Scientific Instruments, Cambridge, UK) attached to a BX51 microscope (Olympus Optical, London, UK) driven by CellP (Soft Imaging System, Munster, Germany). The area of Hoechst 33342 fluorescence as a percentage of the total tumour area (mean Hoechst perfused area (mHPA)) was then calculated using CellP.

Statistics

All data is reported as mean of median values ± 1 standard error of the mean unless otherwise stated. Statistical significance was determined using Student's two-tailed unpaired t-test assuming two samples of the population with equal variance. A p-value of <0.05 was considered significant.

Results

MRI-derived Tumour Volumes

The small tumour cohort of subcutaneous PC3 LN3 xenografts had a mean volume of 44 ± 9 mm^3, which was significantly smaller than the large subcutaneous tumour cohort (563 ± 40 mm^3, $p<0.01$). The orthotopically-propagated PC3 LN3 xenografts had a mean volume of 377 ± 134mm^3.

Quantitation of Tumour R_2, $\Delta R_2^*_{carbogen}$ and Fractional Blood Volume*

Small and large subcutaneous, and orthotopic PC3 LN3 tumours exhibited significantly different mean baseline R_2*, and $\Delta R_2^*_{carbogen}$ (Figures 1a&b). The mean baseline R_2* was

significantly faster in the small subcutaneous tumour cohort than in the large subcutaneous or orthotopic PC3 LN3 tumours, and orthotopic tumours exhibited a significantly slower baseline R_2* than the large subcutaneous tumours. Mean $\Delta R_2^*_{carbogen}$ was negative in the small subcutaneous tumour cohort, and positive in both the large subcutaneous and orthotopic cohorts. The mean fractional tumour blood volume was significantly greater in the small subcutaneous tumours compared to the large subcutaneous and orthotopic tumours (Figure 1c). Fractional blood volume was significantly higher in the orthotopic cohort, compared to the large subcutaneous group.

CUSPIO Imaging Response Categories

Representative CUSPIO RGB maps, which show the spatial distribution of R_2* responses to carbogen breathing and USPIO particle injection, for small and large subcutaneous, and orthotopic PC3 LN3 tumours are shown in Figure 2. Visual inspection of the RGB maps from all tumour cohorts showed a heterogeneous spatial distribution of the five CUSPIO response categories. The RGB maps from each of the PC3 LN3 tumour cohorts revealed a differing spatial distribution of CUSPIO response categories. The large subcutaneous tumours typically showed a central non-responding region, which were less prevalent in the small or orthotopic tumours. Orthotopic tumours appeared to have larger continuous regions of green and cyan voxels contained in one area of the tumour, whereas the subcutaneous tumours exhibited several smaller, more discrete regions of green voxels distributed across the tumour. A greater incidence of yellow voxels was noticeable in the orthotopic tumour RGB maps, compared to the subcutaneous tumour cohorts, which agrees with the quantified CUSPIO data.

The predicted predominant response of tumour tissue to carbogen breathing and USPIO particles is a negative $\Delta R_2^*_{carbogen}$ followed by positive $\Delta R_2^*_{USPIO}$, represented by cyan voxels on the RGB maps. It was therefore interesting that the RGB maps for all the PC3 LN3 tumours showed regions where there was significant $\Delta R_2^*_{carbogen}$ but no significant $\Delta R_2^*_{USPIO}$ (red and blue voxels), and regions where there was no significant $\Delta R_2^*_{carbogen}$ followed by a significant $\Delta R_2^*_{USPIO}$ (green voxels). The CUSPIO response categories in PC3 LN3 prostate tumours were separated spatially into regions that were larger than a single voxel (0.23 × 0.23 mm^2), but small compared to the entire tumour ROI (2).

To quantify the spatial information displayed in the CUSPIO RGB maps, the percentage of tumour ROI voxels that exhibited each R_2* response category was calculated, and is summarised in Table 1. No significant difference in any of the five CUSPIO response

categories was measured between the small and large subcutaneous PC3 LN3 tumour cohorts. A significantly greater percentage of the tumour ROI was occupied by red and yellow voxels in the orthotopic cohort, compared to the small subcutaneous tumours. A significantly smaller number of blue voxels was measured in the orthotopic cohort, compared to the small subcutaneous tumours.

Hoechst 33342 ~~and CD31~~ Fluorescence Microscopy

Composite fluorescence images of Hoechst 33342 uptake from a small and large subcutaneous tumours and an orthotopic PC3 LN3 xenograft are shown in Figure 3a. Hoechst 33342 uptake was heterogeneous in all three tumour cohorts, and visually greater in the centre of the small subcutaneous and orthotopic tumours. Significantly greater mHPA was determined in both the small subcutaneous and orthotopic cohorts compared to the large subcutaneous tumour group (Figure 3b).

Discussion

In this study, the CUSPIO imaging protocol was used to investigate how tumour size and site of implantation affect the vascular characteristics and function of PC3 LN3 prostate tumours *in vivo*. PC3 LN3 prostate tumours were propagated subcutaneously and orthotopically, and the subcutaneous tumours were separated into small and large tumour cohorts. All tumours were then imaged using the CUSPIO imaging protocol. It was hypothesised that tumour size and site of implantation would affect the resulting vascular phenotype.

Tumour Baseline R_2, $\Delta R_2^*{}_{carbogen}$ and Fractional Blood Volume*

As the oxygenation of haemoglobin is proportional to the arterial blood p_aO_2, and therefore in equilibrium with tissue pO_2, measurements of baseline R_2* have been exploited as a sensitive biomarker of hypoxia (11, 24). The significantly faster baseline R_2* determined in the small subcutaneous PC3 LN3 xenografts suggests that tumours from this cohort were the most hypoxic. In order to progress, such small tumours are likely to initiate a strong hypoxia-driven vasculogenic drive, with associated increase expression of VEGF, resulting in immature, unstable vasculature transporting predominantly deoxygenated blood, resulting in a relatively faster R_2*. Magnetic field inhomogeneties arising from susceptibility artefacts caused by air-tissue interfaces, which may be more prevalent when imaging such small tumours, would also impact on the R_2* measurement, though the use of dental paste to immobilise the tumours should limit this (19).

Tumour $\Delta R_2^*_{carbogen}$ was significantly different across all three tumour cohorts, suggesting that both the size and site of implantation of the PC3 LN3 tumours had an effect on their incipient haemodynamic vasculature (25). Differences in functional vasculature between subcutaneous and orthotopic tumours reflects a difference in the interaction of tumour vessels with the host vasculature, or differential pericyte/endothelial cell recruitment by different host tissues (26, 27). Tumour-stromal interactions are powerful determinants of vascular growth factor expression, and therefore the resulting vasculature (26, 28). Furthermore, growth factor receptor expression differs in endothelial cells from different tissues, which may be reflected in these differences in MRI vascular biomarkers (29). Differences between small and large subcutaneous xenografts is likely a consequence of more mature vasculature, higher interstitial pressure and increasing lack of vascular hierarchy associated with larger tumours (30). The small subcutaneous tumour cohort exhibited a negative $\Delta R_2^*_{carbogen}$, indicative of a functional, erythrocyte perfused vascular network (11). Combined with their significantly faster baseline R_2^*, these data suggest that the small PC3 LN3 tumours were hypoxic at baseline, and become less hypoxic during carbogen breathing (31). The positive $\Delta R_2^*_{carbogen}$ measured in the large subcutaneous and orthotopic tumours can be explained by the vascular steal effect, that is the distribution of blood away from the tumour vascular bed by the systemic vasculature (32, 33). From this it can be inferred that both these cohorts have less haemodynamic vasculature than the small subcutaneous tumours.

The significantly greater fractional blood volume in the small subcutaneous PC3 LN3 tumours is consistent with previous work showing that small tumours are often better perfused (30). Vasculogenesis in small tumours provides a nutritive blood supply, but which may not meet the evolving metabolic adaptation/demands of the cancer cells, hence their markedly elevated hypoxia. As tumours progress, their rapid growth outpaces angiogenesis, resulting in a more poorly organised vascular hierarchy which, in conjunction with raised interstitial fluid pressure, causes plasma perfusion as a percent of tumour volume to decrease (27). Hoechst 33342 uptake showed close agreement with the MRI derived fractional blood volume results from the same subcutaneous tumours, providing further validation of this imaging biomarker (34, 35). Orthotopic PC3 LN3 tumours exhibited a significantly larger blood volume than the large subcutaneous tumours, reflecting differences in vascular phenotype associated with the different tumour microenvironments, as there was no significant difference in the mean volumes of these tumour cohorts. This is consistent with the elevated vascular volume, measured by MRI, in orthotopic, compared to subcutaneous, PC3 tumours (36). These differences may arise from tumour cell interactions

with stromal cells from the prostate compared to dermal site, or because of differential angiogenic growth factor receptor expression in the different tissues.

CUSPIO Imaging

The CUSPIO RGB maps from all three PC3 LN3 tumour cohorts revealed regions where R_2* changed significantly (+ or -) during carbogen breathing, but did not change after administration of USPIO particles (blue and red voxels), as previously observed in other tumour models (2). This suggests these regions have experienced vascular shutdown in the 15 minute period between carbogen inhalation and injection of USPIO particles. RGB maps from all tumours also showed a heterogeneous spatial distribution of $\Delta R_2^*_{USPIO}$ (green) voxels, which is indicative of heterogeneous plasma perfusion. Green CUSPIO voxels have been previously shown to have a close spatial association with Hoechst 33342 uptake (2). RGB maps from the orthotopic PC3 LN3 tumours showed localised regions of green and cyan voxels, compared to more heterogeneous distribution seen in the subcutaneous tumours. This may reflect a difference in vascular supply to the tumours, resulting from the different microenvironments (9).

There was no significant difference in any of the CUSPIO ΔR_2* response categories between the small and large subcutaneous tumours, suggesting a similar incidence of transient hypoxia and levels of plasma perfusion in these two cohorts. Tumour size may therefore only weakly influence the incidence of intermittent blood flow and plasma perfusion, compared to tumour-stroma interactions and the effect of site of implantation. The similarity in the yellow and cyan CUSPIO response categories in the small and large tumours suggests that these two models had similarly patent, functional vasculature.

Quantitation of the CUSPIO categories revealed that orthotopic PC3 LN3 tumours exhibited a significantly greater percentage of red and yellow voxels, and a significantly smaller number of blue voxels, than the small subcutaneous cohort. The lower number of blue voxels suggests a lower incidence of transient hypoxia in the orthotopic tumours. The greater number of yellow voxels also suggests the orthotopic tumours experienced a lower incidence of intermittent blood flow, as more of the tumour remained perfused throughout the whole CUSPIO imaging session compared to the small subcutaneous tumours. The greater percentage of red voxels, combined with the higher incidence of yellow voxels, in the orthotopic tumours, may indicate a greater incidence of vascular steal. This inference aligns with the positive mean $\Delta R_2^*_{carbogen}$ measured in the orthotopic tumours, compared to the negative mean $\Delta R_2^*_{carbogen}$ measured in the small subcutaneous cohort. Numerous factors

are important determinants of the vascular phenotype that develops in tumours, including vascular endothelial growth factor (VEGF) expression, endothelial cell VEGF receptor expression, and platelet-derived growth factor receptor (PDGFR-β) expression, and are all influenced by tumour-stroma interactions. The differences in CUSPIO response categories measured between small subcutaneous and orthotopic PC3 LN3 tumours may therefore reflect differences in pericyte coverage and vascular density in these two models, and which may also be influenced by the vascular bed at each anatomical site (26, 28, 37, 38).

Efficient tumour plasma perfusion is a key determinant of drug delivery, so a clear understanding on the extent, patency and spatial distribution of functional tumour vasculature *in vivo* provided by techniques such as CUSPIO imaging is imperative for appropriate tumour model selection when designing pre-clinical therapy trials. Carbogen inhalation has been used both clinically and pre-clinically to increase drug uptake, in solid tumours through hypercapnia-induced vasodilation (39-43). The potential to use CUSPIO imaging to non-invasively assess the degree and heterogeneity of vascular functionality, tumour oxygenation and vascular shutdown will impact on both chemotherapy and radiotherapy, which generally exhibit higher efficacy in well oxygenated tumour tissue (44). Differences in vascular architecture and function arising in subcutaneous and orthotopic models also has implications for the sensitivity of a model in which to evaluate novel anti-angiogenic drugs, and targeted agents whose mode of action is predicted to elicit an anti-angiogenic effect (3).

In conclusion, the vascular structure and function of tumour xenografts, derived from a PC3 LN3 human prostate cell line, was shown to be dependent on both the site of implantation and relative tumour size using the CUSPIO imaging protocol. Significant differences in $\Delta R_2^*{}_{carbogen}$, fractional blood volume and CUSPIO response categories were determined between small and large subcutaneous, and orthotopically propagated PC3 LN3 prostate cancer xenografts.

References

1. Jung CW, Jacobs P. Physical and chemical properties of superparamagnetic iron oxide MR contrast agents: ferumoxides, ferumoxtran, ferumoxsil. *Magn Reson Imaging* 1995;13:661-74.

2. Burrell JS, Walker-Samuel S, Baker LC, et al. Investigating temporal fluctuations in tumor vasculature with combined carbogen and ultrasmall superparamagnetic iron oxide particle (CUSPIO) imaging. *Magn Reson Med* 2011;66:227-34.

3. Burrell JS, Walker-Samuel S, Baker LCJ, et al. Evaluation of novel combined carbogen USPIO (CUSPIO) imaging biomarkers in assessing the antiangiogenic effects of cediranib (AZD2171) in rat C6 gliomas. *Int J Cancer* 2012;131:1854-62.

4. Ellis LM, Fidler IJ. Finding the tumor copycat. Therapy fails, patients don't. *Nat Med* 2010;16:974-5.

5. Van Dyke T. Finding the tumor copycat: Approximating a human cancer. *Nat Med* 2010;16:976-7.

6. de Bono JS, Ashworth A. Translating cancer research into targeted therapeutics. *Nature* 2010;467:543-9.

7. Workman P, Aboagye EO, Balkwill F, et al. Guidelines for the welfare and use of animals in cancer research. *Br J Cancer* 2010;102:1555-77.

8. Chesler L, Weiss WA. Genetically engineered murine models – Contribution to our understanding of the genetics, molecular pathology and therapeutic targeting of neuroblastoma. *Semin Cancer Biol* 2011;21:245-55.

9. Walker-Samuel S, Boult JK, McPhail LD, et al. Non-invasive in vivo imaging of vessel calibre in orthotopic prostate tumour xenografts. *Int J Cancer* 2011.

10. Jamin Y, Glass L, Hallsworth A, et al. Intrinsic susceptibility MRI identifies tumors with *ALK*^{F1174L} mutation in genetically-engineered murine models of high-risk neuroblastoma. *PLoS ONE* 2014;9:e92886.

11. Robinson SP, Rijken PF, Howe FA, et al. Tumor vascular architecture and function evaluated by non-invasive susceptibility MRI methods and immunohistochemistry. *J Magn Reson Imaging* 2003;17:445-54.

12. Robinson SP, Ludwig C, Paulsson J, et al. The effects of tumor-derived platelet-derived growth factor on vascular morphology and function *in vivo* revealed by susceptibility MRI. *Int J Cancer* 2008;122:1548-56.

13. Baker LCJ, Boult JKR, Walker-Samuel S, et al. The HIF-pathway inhibitor NSC-134754 induces metabolic changes and anti-tumour activity while maintaining vascular function. *Br J Cancer* 2012;106:1638-47.

14. Boult JKR, Jamin Y, Jacobs V, et al. False-negative MRI biomarkers of tumour response to targeted cancer therapeutics. *Br J Cancer* 2012;106:1960-6.

15. Ramasawmy R, Campbell-Washburn AE, Wells JA, et al. Hepatic arterial spin labelling MRI: an initial evaluation in mice. *NMR Biomed* 2015;28:272-80.

16. Sanderson S, Valenti M, Gowan S, et al. Benzoquinone ansamycin heat shock protein 90 inhibitors modulate multiple functions required for tumor angiogenesis. *Mol Cancer Ther* 2006;5:522-32.

17. Workman P, Aboagye EO, Balkwill F, et al. Guidelines for the welfare and use of animals in cancer research. *Br J Cancer* 2010;102:1555-77.

18. Kilkenny C, Browne WJ, Cuthill IC, et al. Improving bioscience research reporting: The ARRIVE guidelines for reporting animal research. *PLoS Biol* 2010;8:e1000412.

19. Landuyt W, Sunaert S, Farina D, et al. In vivo animal functional MRI: Improved image quality with a body-adapted mold. *J Magn Reson Imaging* 2002;16:224-7.

20. Walker-Samuel S, Orton M, McPhail LD, et al. Bayesian estimation of changes in transverse relaxation rates. *Magn Reson Med* 2010;64:914-21.

21. Yablonskiy DA, Haacke EM. Theory of NMR signal behavior in magnetically inhomogeneous tissues: the static dephasing regime. *Magn Reson Med* 1994;32:749-63.

22. Tropres I, Grimault S, Vaeth A, et al. Vessel size imaging. *Magn Reson Med* 2001;45:397-408.

23. Smith KA, Hill SA, Begg AC, et al. Validation of the fluorescent dye Hoechst 33342 as a vascular space marker in tumours. *Br J Cancer* 1988;57:247-53.

24. McPhail LD, Robinson SP. Intrinsic susceptibility MR imaging of chemically induced rat mammary tumors: relationship to histologic assessment of hypoxia and fibrosis. *Radiology* 2010;254:110-8.

25. Robinson SP, Rijken PF, Howe FA, et al. Tumor vascular architecture and function evaluated by non-invasive susceptibility MRI methods and immunohistochemistry. *J Magn Reson Imaging* 2003;17:445-54.

26. Pietras K, Ostman A. Hallmarks of cancer: interactions with the tumor stroma. *Exp Cell Res* 2010;316:1324-31.

27. Gilead A, Meir G, Neeman M. The role of angiogenesis, vascular maturation, regression and stroma infiltration in dormancy and growth of implanted MLS ovarian carcinoma spheroids. *Int J Cancer* 2004;108:524-31.

28. Fukumura D, Xavier R, Sugiura T, et al. Tumor induction of VEGF promoter activity in stromal cells. *Cell* 1998;94:715-25.

29. Fidler IJ, Ellis LM. The implications of angiogenesis for the biology and therapy of cancer metastasis. *Cell* 1994;79:185-8.

30. Jain RK, Baxter LT. Mechanisms of heterogeneous distribution of monoclonal antibodies and other macromolecules in tumors: significance of elevated interstitial pressure. *Cancer Res* 1988;48:7022-32.

31. Baker LCJ, Boult JKR, Jamin Y, et al. Evaluation and immunohistochemical qualification of carbogen-Induced ΔR_2^* as a noninvasive imaging biomarker of improved tumor oxygenation. *Int J Radiat Oncol Biol Phys* 2013;87:160-7.

32. Karczmar GS, River JN, Li J, et al. Effects of hyperoxia on T2* and resonance frequency weighted magnetic resonance images of rodent tumours. *NMR Biomed* 1994;7:3-11.

33. Robinson SP, Rodrigues LM, Ojugo AS, et al. The response to carbogen breathing in experimental tumour models monitored by gradient-recalled echo magnetic resonance imaging. *Br J Cancer* 1997;75:1000-6.

34. Robinson SP, Howe FA, Griffiths JR, et al. Susceptibility contrast magnetic resonance imaging determination of fractional tumor blood volume: a noninvasive imaging

biomarker of response to the vascular disrupting agent ZD6126. *Int J Radiat Oncol Biol Phys* 2007;69:872-9.

35. Walker-Samuel S, Boult JKR, McPhail LD, et al. Non-invasive in vivo imaging of vessel calibre in orthotopic prostate tumour xenografts. *Int J Cancer* 2012;130:1284-93.

36. Penet M-F, Pathak AP, Raman V, et al. Noninvasive multiparametric imaging of metastasis-permissive microenvironments in a human prostate cancer xenograft. *Cancer Res* 2009;69:8822-9.

37. Pasqualini R, Ruoslahti E. Organ targeting in vivo using phage display peptide libraries. *Nature* 1996;380:364-6.

38. Aird WC. Endothelial cell heterogeneity. *Crit Care Med* 2003;31:S221-30.

39. McSheehy PM, Port RE, Rodrigues LM, et al. Investigations in vivo of the effects of carbogen breathing on 5-fluorouracil pharmacokinetics and physiology of solid rodent tumours. *Cancer Chem Pharm* 2005;55:117-28.

40. McSheehy PM, Robinson SP, Ojugo AS, et al. Carbogen breathing increases 5-fluorouracil uptake and cytotoxicity in hypoxic murine RIF-1 tumors: a magnetic resonance study in vivo. *Cancer Res* 1998;58:1185-94.

41. Gupta N, Saleem A, Kotz B, et al. Carbogen and nicotinamide increase blood flow and 5-fluorouracil delivery but not 5-fluorouracil retention in colorectal cancer metastases in patients. *Clin Cancer Res* 2006;12:3115-23.

42. Rodrigues LM, Maxwell RJ, McSheehy PM, et al. In vivo detection of ifosfamide by 31P-MRS in rat tumours: increased uptake and cytotoxicity induced by carbogen breathing in GH3 prolactinomas. *Br J Cancer* 1997;75:62-8.

43. Rodrigues LM, Robinson SP, McSheehy PM, et al. Enhanced uptake of ifosfamide into GH3 prolactinomas with hypercapnic hyperoxic gases monitored in vivo by (31)P MRS. *Neoplasia* 2002;4:539-43.

44. Kirkpatrick JP, Cardenas-Navia LI, Dewhirst MW. Predicting the effect of temporal variations in PO2 on tumor radiosensitivity. *Int J Radiat Oncol Biol Phys* 2004;59:822-33.

Figure Legends

Figure 1 – Summary of a) baseline R_2*, b) carbogen-induced ΔR_2* and c) fractional blood volume determined from the cohorts of small (n=6) and large (n=6) subcutaneous, and orthotopically propagated PC3 LN3 prostate cancer xenografts (n=5). Values are mean ± 1 s.e.m, *p< 0.05, Student's two tailed unpaired t-test.

Figure 2 – CUSPIO RGB maps from the three axial slices obtained from representative a) small subcutaneous, b) large subcutaneous and c) orthotopic PC3 LN3 prostate xenografts. The key shows the colour-coded CUSPIO response categories.

Figure 3 – a) Composite fluorescence microscopy images showing Hoechst 33342 uptake in represetative small and large subcutaneous, and orthotopic PC3 LN3 prostate xenografts. b) Summary of Hoechst 33342 perfused area (HPA %), which represents plasma perfusion, measured by fluorescence microscopy in small (n=6) and large (n=6) subcutaneous, and orthotopic (n=5) PC3 LN3 prostate tumours. Values are mean ± 1 s.e.m., *p< 0.05, Student's two tailed unpaired t-test.

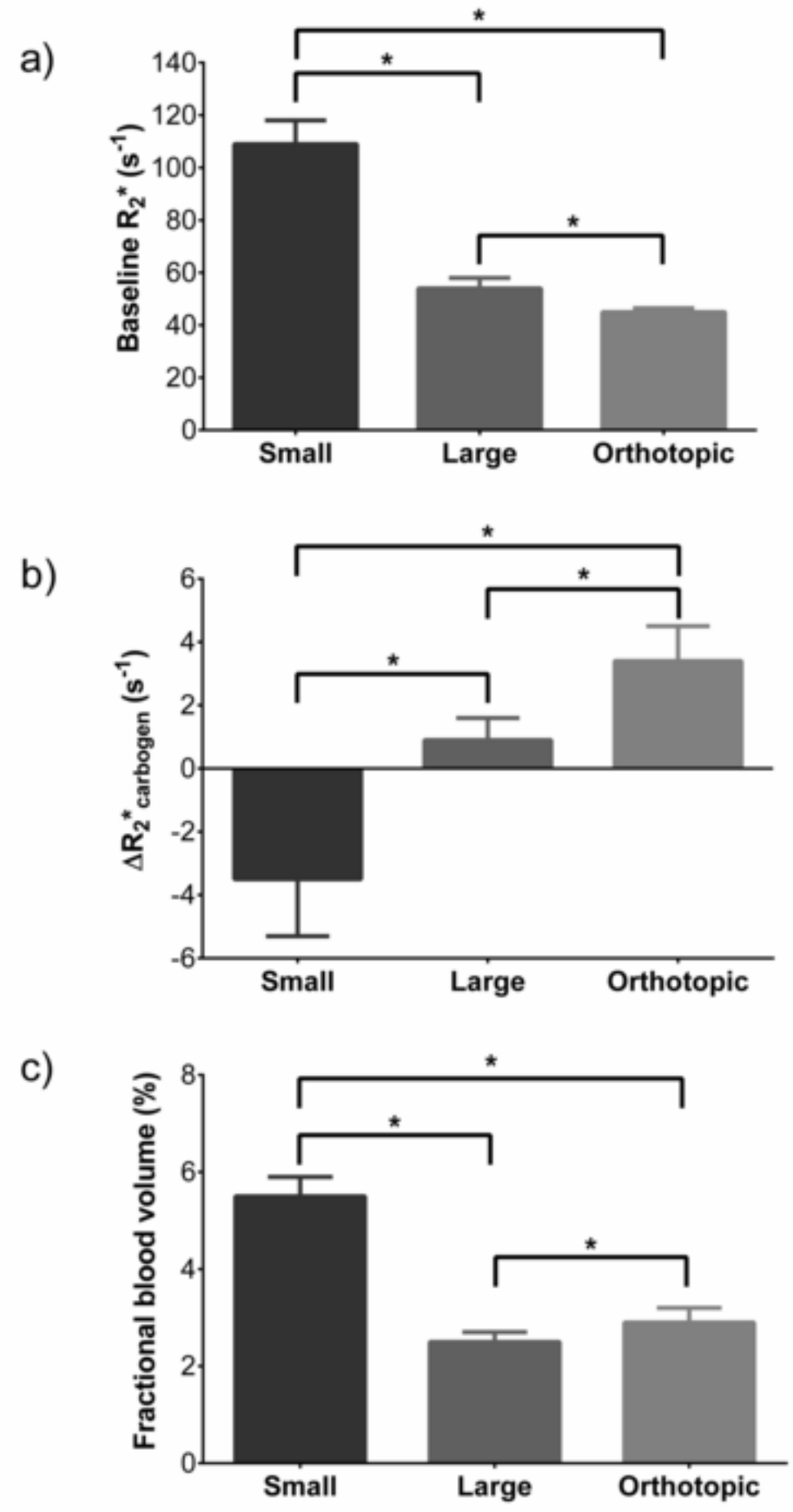

Figure (TIF or EPS only. 300 ppi Images and 1200 ppi Line-art. NO JPEGS)

Click here to download Figure (TIF or EPS only. 300 ppi Images and 1200 ppi Line-art. NO JPEGS) Figure 2.tif

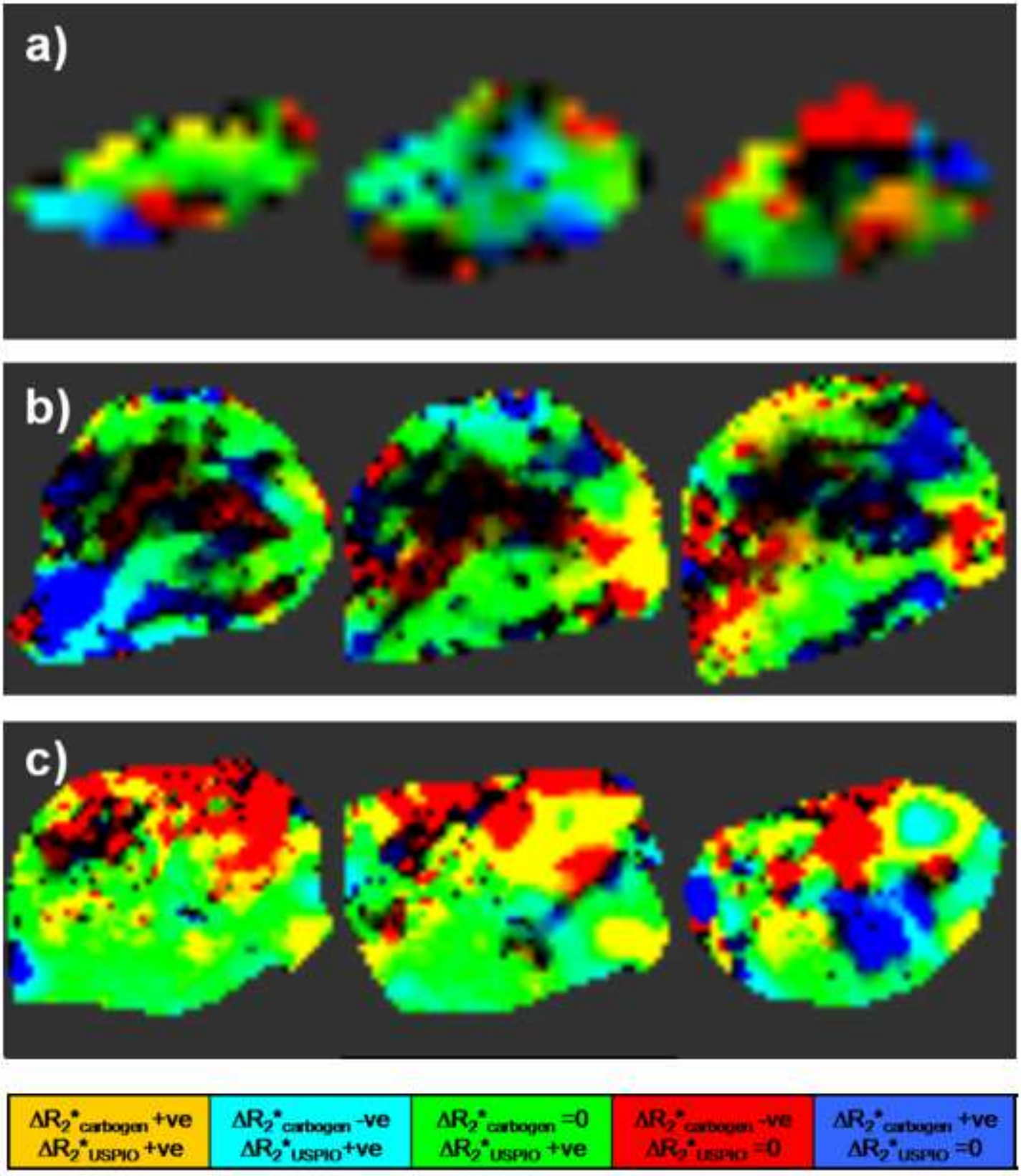

Figure (TIF or EPS only. 300 ppi Images and 1200 ppi Line-art. NO JPEGS)

Click here to download Figure (TIF or EPS only. 300 ppi Images and 1200 ppi Line-art. NO JPEGS) Figure 3a.tif

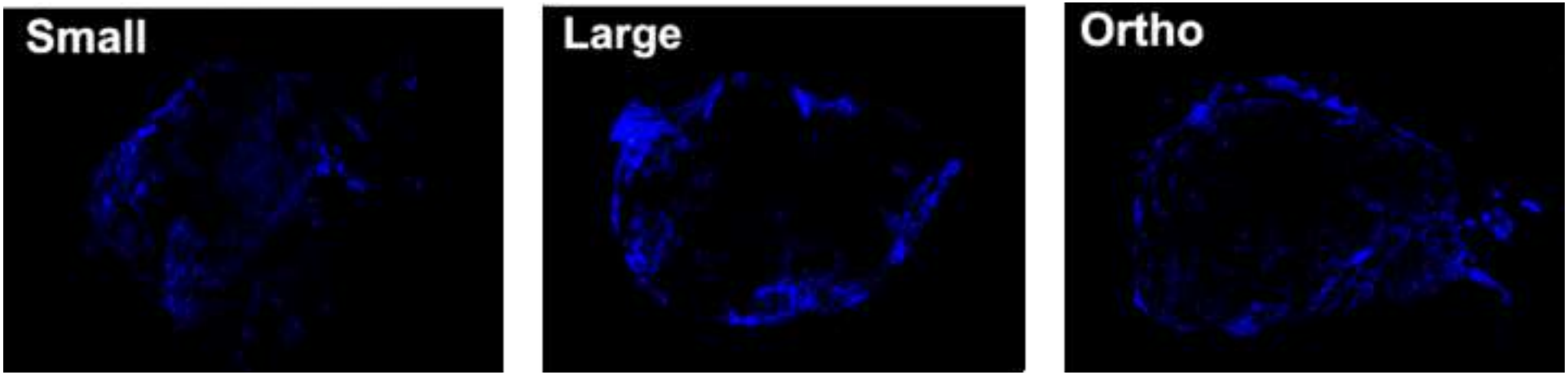

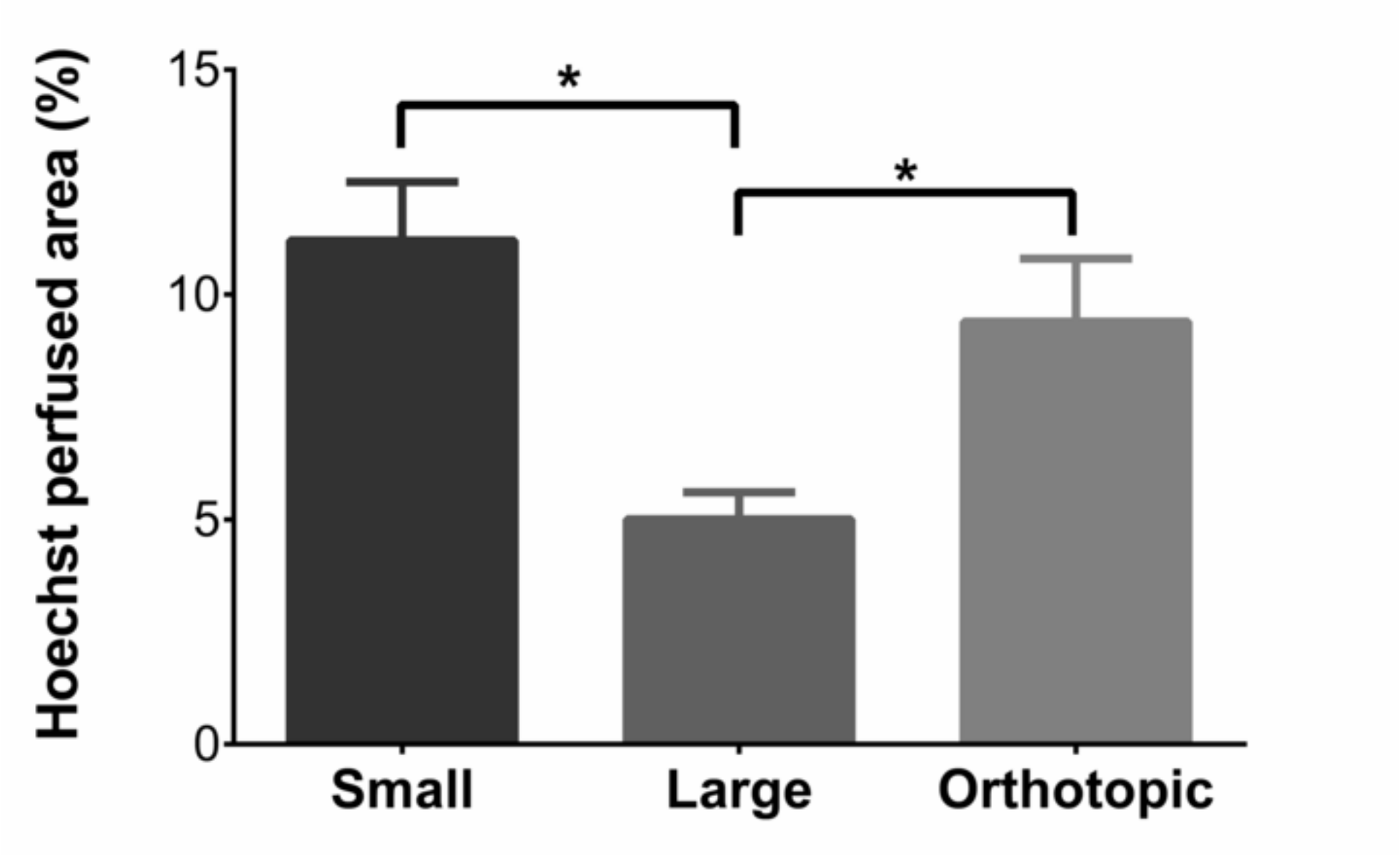

Figure (TIF or EPS only. 300 ppi Images and 1200 ppi Line-art.
NO JPEGS)

Table & Legend

	$\Delta R_2^*{}_{carbogen}$ +ve $\Delta R_2^*{}_{USPIO}$ +ve	$\Delta R_2^*{}_{carbogen}$ -ve $\Delta R_2^*{}_{USPIO}$+ve	$\Delta R_2^*{}_{carbogen}$ =0 $\Delta R_2^*{}_{USPIO}$ +ve	$\Delta R_2^*{}_{carbogen}$ -ve $\Delta R_2^*{}_{USPIO}$ =0	$\Delta R_2^*{}_{carbogen}$ +ve $\Delta R_2^*{}_{USPIO}$ =0
Small	10.1 ± 5	14.3 ± 4	22.2 ± 6	10.9 ± 5	17.5 ± 5
Large	11.1 ± 1	9.0 ± 2	25.8 ± 4	14.0 ± 3	9.6 ± 2
Orthotopic	26.8 ± 5*	11.0 ± 2	22.5 ± 3	17.7 ± 3*	5.9 ± 2*

Table 1 - CUSPIO mean fractional response categories for small and large subcutaneous, and orthotopic PC3 LN3 prostate tumours. Values are mean % of the total tumour ROI ± 1 s.e.m. *p <0.05, Student's two tailed unpaired t-test, between small and orthotopic tumours.